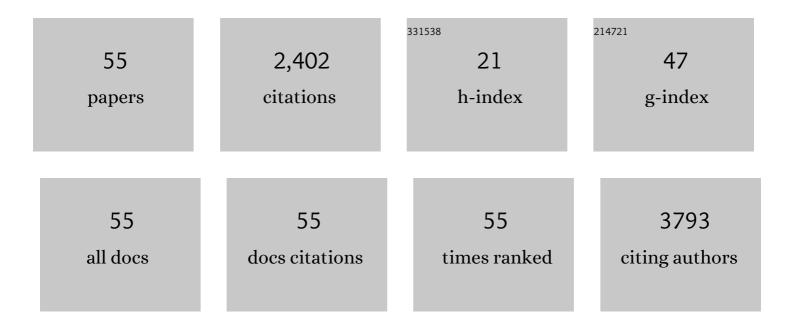
Sung-Il Baik

List of Publications by Year in descending order

Source: https://exaly.com/author-pdf/7079198/publications.pdf Version: 2024-02-01



SUNC-LI RAIK

#	Article	IF	CITATIONS
1	Nonblinking and Nonbleaching Upconverting Nanoparticles as an Optical Imaging Nanoprobe and T1 Magnetic Resonance Imaging Contrast Agent. Advanced Materials, 2009, 21, 4467-4471.	11.1	548
2	Synthesis of Quantum-Sized Cubic ZnS Nanorods by the Oriented Attachment Mechanism. Journal of the American Chemical Society, 2005, 127, 5662-5670.	6.6	443
3	Synthesis of Uniform Hollow Oxide Nanoparticles through Nanoscale Acid Etching. Nano Letters, 2008, 8, 4252-4258.	4.5	210
4	Solution processing of air-stable molecular semiconducting iodosalts, Cs ₂ SnI _{6â^'x} Br _x , for potential solar cell applications. Sustainable Energy and Fuels, 2017, 1, 710-724.	2.5	174
5	Large-Scale Synthesis of Ultrathin Manganese Oxide Nanoplates and Their Applications to T1 MRI Contrast Agents. Chemistry of Materials, 2011, 23, 3318-3324.	3.2	92
6	Magnetic properties of YIG (Y3Fe5O12) thin films prepared by the post annealing of amorphous films deposited by rf-magnetron sputtering. Journal of Applied Physics, 2005, 97, 10A319.	1.1	82
7	The effect of zirconium on the omega phase in Ti-24Nb-[0–8]Zr (at.%) alloys. Acta Materialia, 2018, 153, 62-70.	3.8	73
8	Precipitation strengthening in naturally aged Al–Zn–Mg–Cu alloy. Materials Science & Engineering A: Structural Materials: Properties, Microstructure and Processing, 2021, 803, 140719.	2.6	65
9	Phase Analysis of Steels by Grain-averaged EBSD Functions. ISIJ International, 2011, 51, 130-136.	0.6	58
10	Grain-boundary structure and segregation behavior in a nickel-base stainless alloy. Scripta Materialia, 2012, 66, 809-812.	2.6	52
11	Increasing the creep resistance of Fe-Ni-Al-Cr superalloys via Ti additions by optimizing the B2/L21 ratio in composite nano-precipitates. Acta Materialia, 2018, 157, 142-154.	3.8	51
12	Deformation behavior of duplex austenite and <i>Ĵµ</i> -martensite high-Mn steel. Science and Technology of Advanced Materials, 2013, 14, 014204.	2.8	39
13	The effect of nitrogen on the stacking fault energy in Fe–15Mn–2Cr–0.6C– x N twinning-induced plasticity steels. Scripta Materialia, 2014, 92, 23-26.	2.6	39
14	A correlative four-dimensional study of phase-separation at the subnanoscale to nanoscale of a Ni Al alloy. Acta Materialia, 2019, 171, 306-333.	3.8	34
15	Room temperature near-ultraviolet emission from In-rich InGaNâ^•GaN multiple quantum wells. Applied Physics Letters, 2005, 86, 192105.	1.5	31
16	Correlative atom-probe tomography and transmission electron microscope study of a chemical transition in a spinel on an oxidized nickel-based superalloy. Scripta Materialia, 2013, 68, 909-912.	2.6	29
17	Effects of Ti addition on the microstructure and mechanical properties of Al–Zn–Mg–Cu–Zr alloy. Materials Science & Engineering A: Structural Materials: Properties, Microstructure and Processing, 2021, 801, 140437.	2.6	29
18	Atom probe tomography study of Fe-Ni-Al-Cr-Ti ferritic steels with hierarchically-structured precipitates. Acta Materialia, 2018, 144, 707-715.	3.8	26

SUNG-IL BAIK

#	Article	IF	CITATIONS
19	Microstructure and creep performance of a multicomponent Co-based L12–ordered intermetallic alloy. Acta Materialia, 2020, 196, 396-408.	3.8	26
20	Temperature increases and thermoplastic microstructural evolution in adiabatic shear bands in a high-strength and high-toughness 10Âwt.% Ni steel. Acta Materialia, 2021, 205, 116568.	3.8	25
21	Grain-boundary structure and segregation in Nb3Sn coatings on Nb for high-performance superconducting radiofrequency cavity applications. Acta Materialia, 2020, 188, 155-165.	3.8	24
22	Quantitative measurement of cementite dissociation in drawn pearlitic steel. Materials Science & Engineering A: Structural Materials: Properties, Microstructure and Processing, 2011, 528, 4947-4952.	2.6	22
23	Effect of hafnium micro-addition on precipitate microstructure and creep properties of a Fe-Ni-Al-Cr-Ti ferritic superalloy. Acta Materialia, 2018, 153, 126-135.	3.8	21
24	In situ observations of transgranular crack propagation in high-manganese steel. Scripta Materialia, 2015, 100, 32-35.	2.6	18
25	Investigation of Strength Recovery in Welds of NUCu-140 Steel Through Multipass Welding and Isothermal Post-Weld Heat Treatments. Metallurgical and Materials Transactions A: Physical Metallurgy and Materials Science, 2015, 46, 5158-5170.	1.1	18
26	Systematic approaches for targeting an atom-probe tomography sample fabricated in a thin TEM specimen: Correlative structural, chemical and 3-D reconstruction analyses. Ultramicroscopy, 2018, 184, 284-292.	0.8	18
27	Enhanced Coarsening Resistance of Q-phase in Aluminum alloys by the addition of Slow Diffusing Solutes. Materials Science & Engineering A: Structural Materials: Properties, Microstructure and Processing, 2018, 735, 318-323.	2.6	18
28	Atomicâ€Scale Structural and Chemical Study of Columnar and Multilayer Re–Ni Electrodeposited Thermal Barrier Coating. Advanced Engineering Materials, 2016, 18, 1133-1144.	1.6	15
29	Evolution of Microstructure and Carbon Distribution During Heat Treatments of a Dual-Phase Steel: Modeling and Atom-Probe Tomography Experiments. Metallurgical and Materials Transactions A: Physical Metallurgy and Materials Science, 2019, 50, 436-450.	1.1	13
30	Crystallographic characterization of Al18Mg3Ti2 intermetallic phase in Al–Zn–Mg–Cu–Zr–Ti alloy. Journal of Alloys and Compounds, 2020, 844, 156173.	2.8	13
31	A transmission electron microscopy and atom-probe tomography study of martensite morphology and composition in a dual-phase steel. Materials Characterization, 2020, 162, 110207.	1.9	13
32	An Atomistic Tomographic Study of Oxygen and Hydrogen Atoms and their Molecules in CVD Grown Graphene. Small, 2015, 11, 5968-5974.	5.2	12
33	Atom-probe tomography of tribological boundary films resulting from boron-based oil additives. Scripta Materialia, 2016, 111, 64-67.	2.6	10
34	Effect of aging on coarsening- and creep resistance of a Ti-modified Fe–Ni–Al–Cr–Mo ferritic steel with L21/B2 composite precipitates. Materials Science & Engineering A: Structural Materials: Properties, Microstructure and Processing, 2020, 776, 138987.	2.6	8
35	Effect of U and Th trace additions on the precipitation strengthening of Al–0.09Sc (at.%) alloy. Journal of Materials Science, 2019, 54, 3485-3495.	1.7	7
36	Galvanic Corrosion Assessment of Friction Stir Butt Welded Joint of Aluminum and Steel Alloys. International Journal of Precision Engineering and Manufacturing - Green Technology, 2020, 7, 905-911.	2.7	7

SUNG-IL BAIK

#	Article	IF	CITATIONS
37	Atom-probe tomographic and dilatometric studies of phase-transformations after inter-critical annealing of a low-carbon dual-phase steel. Materials Characterization, 2020, 168, 110544.	1.9	7
38	Atomically resolved calcium phosphate coating on a gold substrate. Nanoscale, 2018, 10, 8451-8458.	2.8	5
39	Microstructural Investigation of Bilayer Growth of In- and Ga-Rich InGaN Grown by Chemical Vapor Deposition. Journal of Electronic Materials, 2009, 38, 518-522.	1.0	4
40	A transmission electron microscopy study of strain-induced secondary twin and epsilon-martensitic transformation in Fe-15Mn-2Cr-0.6C-0.06N austenitic steel. Materialia, 2020, 10, 100677.	1.3	4
41	The effects of alloying elements on the peritectic range of Fe–C–Mn–Si steels. Journal of Materials Science, 2021, 56, 6448-6464.	1.7	4
42	Microstructural evolution of tantalum nitride thin films synthesized by inductively coupled plasma sputtering. Applied Microscopy, 2020, 50, 7.	0.8	4
43	The effects of diffusional couplings on compositional trajectories and interfacial free energies during phase separation in a quaternary Ni-Al-Cr-Re model superalloy. Acta Materialia, 2022, 234, 118020.	3.8	4
44	Three-Dimensional Atomistic Tomography of W-Based Alloyed Two-Dimensional Transition Metal Dichalcogenides. ACS Applied Materials & amp; Interfaces, 2018, 10, 30640-30648.	4.0	3
45	Analysis of antioxidation behavior of cryo-milled oxide-dispersion-strengthened ferritic steel incorporated with formation of Y–Ti–O(N) nano-precipitates. Acta Materialia, 2022, 225, 117589.	3.8	2
46	Characterization of TaN thin films synthesized by ICP assisted sputtering. Microscopy and Microanalysis, 2008, 14, 330-331.	0.2	1
47	Mn-deprived Phase Transformation in High-Mn Steel during the Dew-point Control Process. Applied Microscopy, 2013, 43, 40-45.	0.8	1
48	Observation of Point Defect in Silicon using HRTEM. Microscopy and Microanalysis, 2004, 10, 994-995.	0.2	0
49	In-Situ Tensile Observation of Deformation Twin in TWIP Steel Using TEM. Microscopy and Microanalysis, 2009, 15, 702-703.	0.2	0
50	An Experimental and Simulation Studies of a High Strain-Rate Deformation Shear Band in a High-Nickel Steel. Microscopy and Microanalysis, 2015, 21, 363-364.	0.2	0
51	The Supersaturation and Transient Volume Measurement for Nucleation, Growth, Coarsening in a Concentrated Ni-Based Superalloy. Microscopy and Microanalysis, 2017, 23, 724-725.	0.2	0
52	The Effects of Diffusional Couplings on Compositional Trajectories and Interfacial Free Energies During Phase Separation in a Quaternary Ni-Al-Cr-Re Model Superalloy. SSRN Electronic Journal, 0, , .	0.4	0
53	Microstructure and Creep Performance of a Multicomponent Co-Based L1 ₂ -Ordered Intermetallic Alloy. SSRN Electronic Journal, 0, , .	0.4	0
54	An Atom-probe Tomographic Study of Kinetic Pathways of Retention Excesses and Depletions at Gamma(F.C.C.)/gamma-prime (L12) Interfaces in a Ni-Al-Cr-Re Superalloy. Microscopy and Microanalysis, 2020, 26, 2076-2076.	0.2	0

#	Article	IF	CITATIONS
55	Temperature Increases and Thermoplastic Microstructural Evolution in Adiabatic Shear-Bands in a High-Strength and High-Toughness 10 wt.% Ni Steel. SSRN Electronic Journal, 0, , .	0.4	0